


## RESEARCH ARTICLE

# High altitude ducts causing abnormal wave propagation in coastal area of Korea

Tae Heung Lim<sup>1</sup> | Sungsik Wang<sup>1</sup> |  
Young-Jun Chong<sup>2</sup> | Yong Bae Park<sup>3</sup> |  
Jinwon Ko<sup>4</sup> | Hosung Choo<sup>1</sup> 

<sup>1</sup>School of Electronic and Electrical Engineering, Hongik University, Seoul, South Korea

<sup>2</sup>Electronics and Telecommunications Research Institute, Broadcasting & Media Laboratory, Daejeon, South Korea

<sup>3</sup>Department of Electrical and Computer Engineering, Ajou University, Suwon, South Korea

<sup>4</sup>Hanwha Systems, AESA Radar R&D Center, Gyeonggi, South Korea

## Correspondence

Hosung Choo, School of Electronic and Electrical Engineering, Hongik University, Seoul, South Korea.

Email: hschoo@hongik.ac.kr

## Abstract

This article analyzes the number of duct occurrences in the Korean coastal area by seasonal statistical histograms using massive atmospheric data sets collected from 2010 to 2017 at four meteorological observatories. In order to estimate electromagnetic wave propagation characteristics in the presence of the duct atmosphere, we obtain and examine the path loss values by using the advanced refractive prediction system (AREPS) software applying the massive refractive index data set and the actual Korean coastal terrain data. These results are then fitted using Burr Type XII PDF curves to derive quantitative mean and variance values. To verify the suitability of the simulated path losses in the proposed analysis, the measurement of the path losses between Jeung-do and Heuksan-do are carried out in October 2017. The measurements and simulations of the autumn results are fitted by Burr Type XII CDF curves and agree well with each other.

## KEYWORDS

duct, propagation interference, refractive index, trilinear modeling

## 1 | INTRODUCTION

Wireless communication technologies using electromagnetic (EM) waves have been extended not only in short-range applications such as two-way radios, mobile phones, Bluetooth, and wireless fidelity (Wi-Fi) but also in long distance applications such as broadcasting radio, point-to-point microwave communications, satellite communications, and even deep space communications.<sup>1-3</sup> The long-range wireless communication systems have undesired deterioration in communication performance due to abnormal EM characteristics, such as clutters, thermal noises, vapors, and variations of atmospheric refractivity.<sup>4</sup> Among them, the atmospheric refractivity can have a significant impact on the EM wave propagation, and thus high-altitude atmospheric conditions are classified into four conditions: normal, sub, super, and duct.<sup>5</sup> Most abnormal wave propagation characteristics are often observed under the duct atmosphere, and the ducts frequently occur in coastal areas because of a temperature inversion between the warm and cold air layers,<sup>6</sup> a rapid decrease of humidity along the altitude,<sup>7</sup> or a change of water vapor content in the sea surface.<sup>8</sup> Therefore, recently, a number of studies have been made to estimate such duct conditions using refractivity index based on the measured path loss, for example, path loss measurement in turbulence media,<sup>9</sup> measurement of sea surface reflected clutter signals,<sup>10-14</sup> and observing the tropospheric delay at the global positioning systems.<sup>15-17</sup> Many countries such as the United States,<sup>18</sup> Europe,<sup>19</sup> and China<sup>20</sup> have investigated abnormal wave propagation characteristics under duct atmosphere in their coastal areas. However, most of these studies have focused on demonstrating the abnormal wave propagation in duct conditions and have not yet sufficiently considered the seasonal frequency, altitude, and thickness of the occurred ducts in coastal areas. Especially, in case of Korea that has many coastal areas surrounded by sea, the occurrence of abnormal wave propagations by the duct atmosphere are more commonly encountered, but in-depth investigations have not been conducted on these duct characteristics so far.

In this article, the number of duct occurrences in Korean coastal area is analyzed seasonally by statistical histograms using massive atmospheric data sets collected from 2010 to 2017 at four meteorological observatories. In addition, the duct characteristics of the occurring altitude and thickness are calculated from the data sets in order to examine seasonal duct properties. Then, to estimate EM wave propagation characteristics in various atmospheric environments, the

path loss values are obtained and examined by using the advanced refractive prediction system (AREPS) software<sup>21</sup> based on a hybrid model<sup>22-24</sup> where the massive refractivity data set and the digital terrain elevation data (DTED) between Jeung-do and Heuksan-do in Korean coastal area are given as inputs to the software. To observe duct effects, the seasonal path losses are divided into the presence and absence of atmospheric ducts and compared to each other. These results are fitted using Burr Type XII probability density function (PDF) curves to derive quantitative mean and variance values depending on the presence of the duct. To verify the suitability of the simulated path loss in the proposed analysis, the path losses between Jeung-do and Heuksan-do are measured in October 2017, and these results are compared to the simulation.

## 2 | STATISTICAL DUCT CHARACTERISTIC ANALYSIS USING MASSIVE ATMOSPHERIC DATA SETS

Figure 1 shows the modified refractivity (M-unit) along the altitude for the surface and elevated ducts where the negative gradient region of the refractivity indicates the trapping layer, where the equation of the modified refractivity  $M$  is defined by adding the ratio of the height  $h$  (km) to the ground curvature with the refractive index  $n$  as follows:

$$M = (n - 1) \times 10^6 + 157h \quad (1)$$

As shown in Figure 1A, in the surface duct, the duct thickness is defined as the height from the ground to the top of the trapping layer. On the other hand, in the elevated duct as shown in Figure 1B, the thickness of the duct is determined by the height difference between the top of the trapping layer and the lower point with the same refractivity at the top of the trapping layer. The duct height is then denoted by the distance from ground to the bottom of the trapping layer.

In the Korean Peninsula surrounded by three sides of the sea, these kinds of ducting phenomena are consistently and frequently experienced over many years, which causes the abnormal wave propagation characteristics in long-distance wave transmission. In order to statistically observe the duct characteristics causing abnormal wave propagations, we collect massive atmospheric data sets from 2010 to 2017 at four meteorological observatories near the south coast of Korea; Pohang, Chang Won, Heuksan-do, and Gosan, as illustrated with blue circles in Figure 2. The atmospheric data sets include the measured relative humidity, air pressure, and temperature along the altitude, which can be applied to the appropriate equation to achieve the refractive index.<sup>15</sup> According to the southern coastal area of South Korea, the refractivity is first assumed to be locally constant in vicinity of four different meteorological observatories.

However, the refractivity indices obtained from the four meteorological observatories do not have a dense data set or a constant separation distance along the altitude, making statistically data processing difficult. Thus, among many interpolation methods,<sup>25</sup> a basic interpolation of the linear method is applied between the usable data to gradually fill

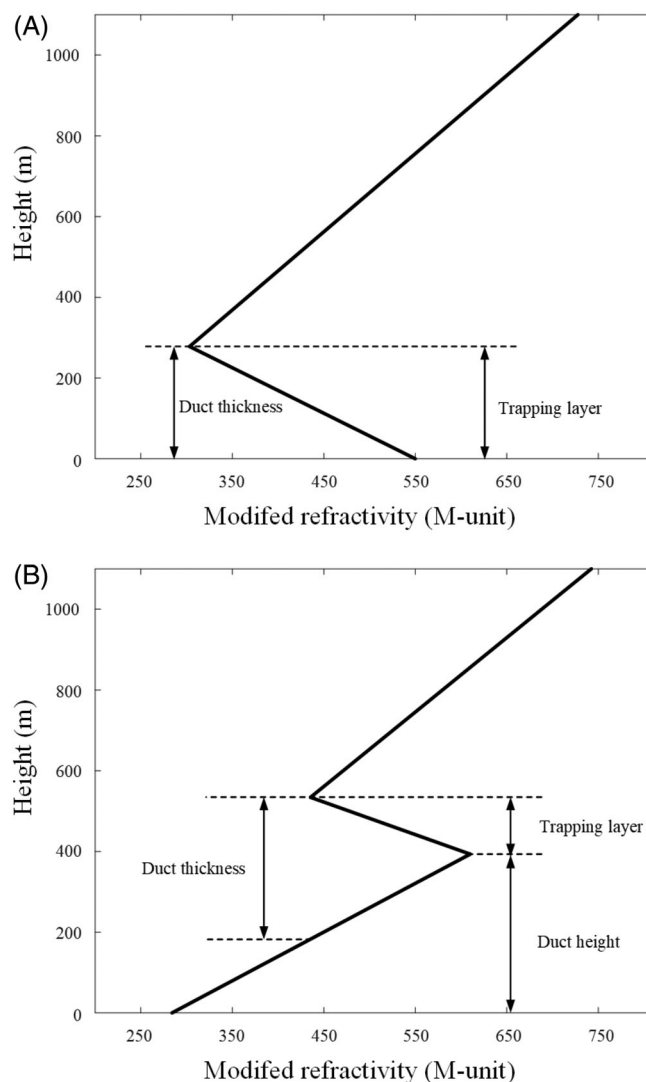


**FIGURE 1** Modified atmospheric refractivity according to altitude. A, Surface duct. B, Elevated duct

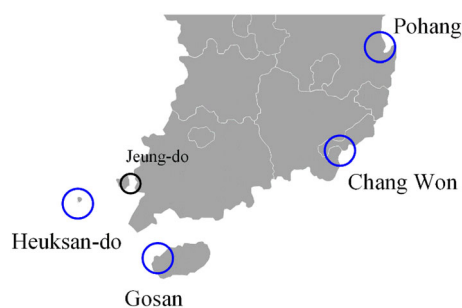


**FIGURE 2** Four meteorological observatories along the south coast of Korea [Color figure can be viewed at wileyonlinelibrary.com]

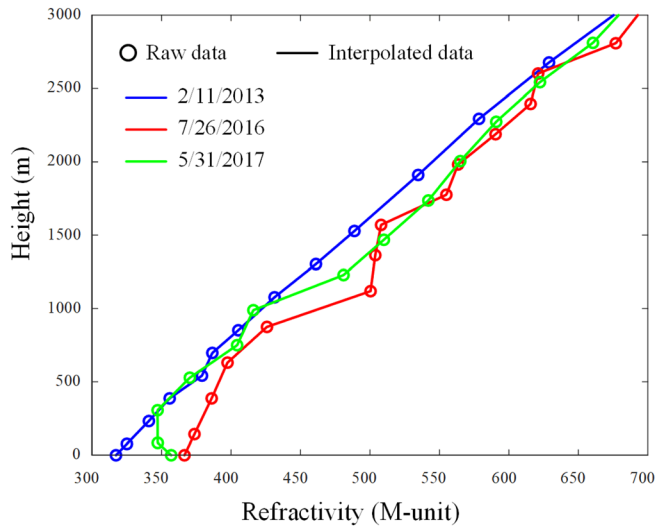


**FIGURE 3** Examples of the comparison between the interpolated and raw refractivity data [Color figure can be viewed at [wileyonlinelibrary.com](http://wileyonlinelibrary.com)]

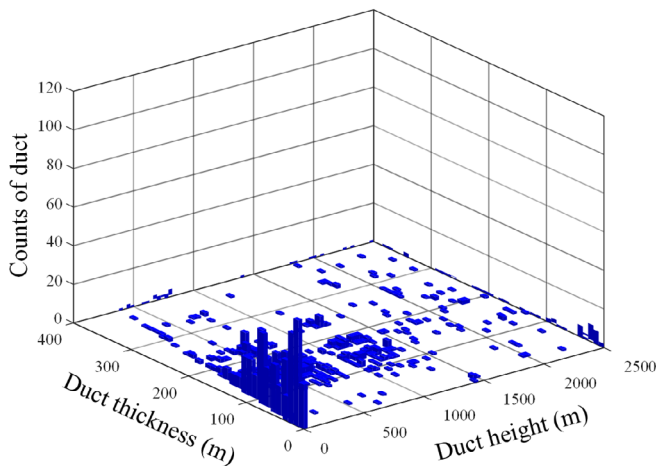


**FIGURE 4** Histogram of the spring atmospheric data according to duct thickness and height [Color figure can be viewed at [wileyonlinelibrary.com](http://wileyonlinelibrary.com)]

the sparse data sets. In addition, missing data at the low altitude is extrapolated using the same gradient of the refractivity at the end point of the data. Finally, the given sparse data sets are uniformly extended to 601 points along the altitude from 0 to 3000 m to investigate duct characteristics more thoroughly. To verify the interpolated results, Figure 3 shows examples of the comparison between the raw and interpolated refractivity data sets, where circular markers and solid lines indicate the raw and interpolated data. The blue, red, and green colors specify the dates and site information for 2/11/2013 (Pohang, 47 138), 7/26/2016 (Chang Won, 47 155), and 5/31/2017 (Heuksan-do, 47 169), respectively. As a result of observation, the raw data are considered to be dense enough to be recovered as reliable interpolated meta profile. Since the four seasons are very distinctive in Korea, the massive data sets are classified into four seasons: spring (3/1 ~ 5/31), summer

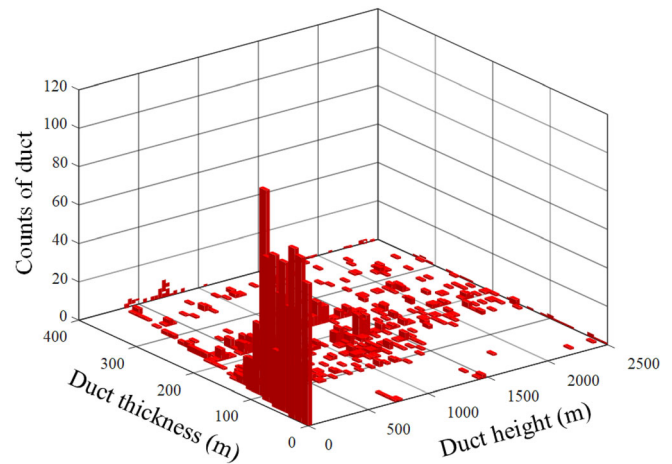


**FIGURE 5** Histogram of the summer atmospheric data according to duct thickness and height [Color figure can be viewed at [wileyonlinelibrary.com](http://wileyonlinelibrary.com)]

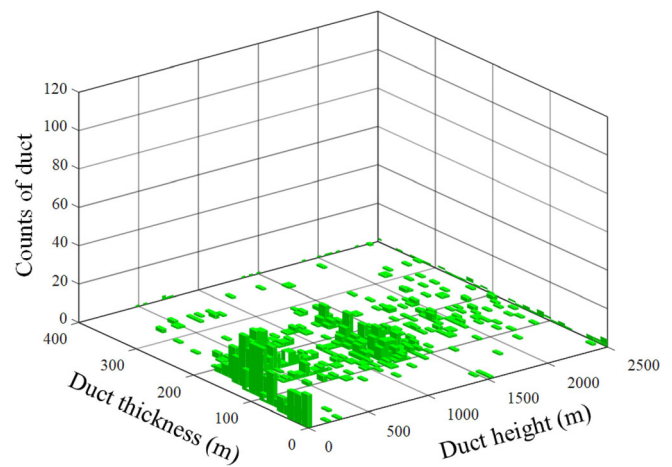


**FIGURE 6** Histogram of the autumn atmospheric data according to duct thickness and height [Color figure can be viewed at [wileyonlinelibrary.com](http://wileyonlinelibrary.com)]

(6/1 ~ 8/31), autumn (9/1 ~ 10/30), and winter (11/1 ~ 2/28). From each seasonal data set, we calculate the gradient of the refractivity indices according to the heights, and the locations of the minus gradient values are found to acquire the heights and thicknesses of the duct. The number of occurrences for the duct is sorted for the surface duct and the elevated duct, respectively. These two duct parameters of the thickness and height with the number of occurrences are statistically analyzed to examine the particular duct characteristics for each season in the Korean coastal area.

Figures 4–7 depict statistical histograms according to the duct thickness and height for each season, where the color bars of blue, red, green, and magenta indicate the spring, summer, autumn, and winter. The total number of bins is fixed at 95 to make a fair comparison of seasonal histograms.

In accordance with the spring data, ducts occurred 1063 times among the entire spring data of 4671, in which the surface duct is predominant with the thickness from 9 to

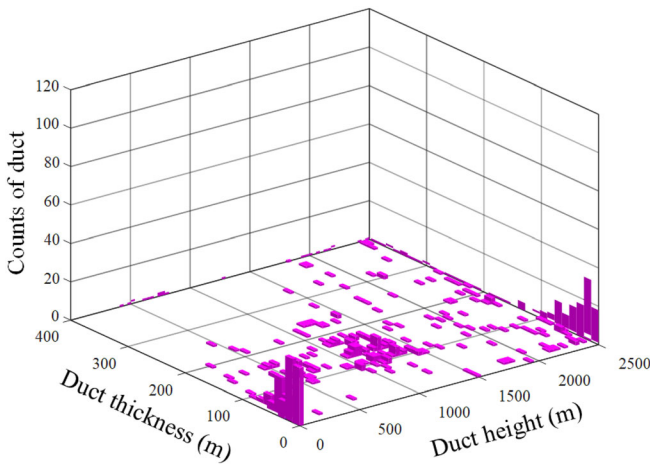


**FIGURE 7** Histogram of the winter atmospheric data according to duct thickness and height [Color figure can be viewed at wileyonlinelibrary.com]

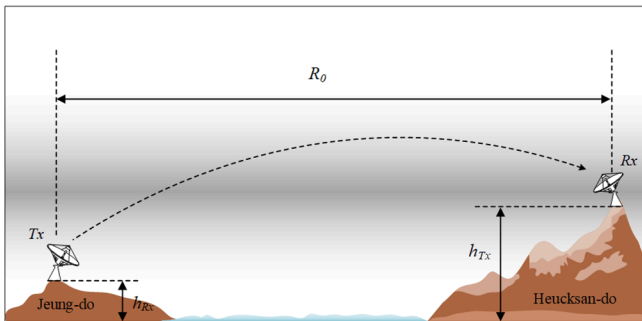


**FIGURE 8** Geometry between Jeung-do and Heuksan-do transceivers located along the Korean coast [Color figure can be viewed at wileyonlinelibrary.com]

128.2 m as shown in Figure 4. It is because the spring has a stable atmosphere with low up-down convections due to high pressure and dry weather, which can reduce the elevated duct occurrences at high altitudes with steady increasing refractivity along the altitude. In contrast, Figure 5 presents the summer data histogram, where the number of the duct occurrences is 1639, about 600 times larger than those of spring, and most surface duct thicknesses are less than 163.8 m, and the heights are under 189.6 m. In terms of the physical phenomenon, the atmospheric conditions are very irregular since high temperature and inconsistent humidity with the altitude can change the refractivity indices to drastically increase the number of duct occurrences. In the autumn season of Figure 6, the duct distribution spreads evenly at the height from the 9 to 1580 m, where the duct occurs 1050 times in the Korean coastal area because the atmospheric conditions is similar to the spring. On the other hand, the winter has the most stable atmosphere among four seasons because the low temperature and the balanced humidity allow for little up-down convection and steady refractivity index. Accordingly, this stable environment can induce the minimum number of ducts occurrences as shown

Figure 7, which is 612 times out of the total winter data sets of 4468. These statistical results confirm the distinctive duct characteristics of thickness and height for each season in the Korean coastal area, and it can be also predicted from the results that many abnormal wave propagations can be encountered in summer.

### 3 | DUCT ANALYSIS USING SIMULATED AND MEASURED PATH LOSS

In the previous chapter, the seasonal duct characteristics were statistically interpreted as the height and the thickness using the massive refractive index data sets. In this chapter, we examine the path loss values using the AREPS software based on the four seasonal refractive index data sets and the actual DTED of the Korean coastal areas to estimate EM wave propagation characteristics in various atmospheric environments. The digital terrain data between Jeung-do and Heuksan-do in the Korean coastal areas extracted from Google Earth,<sup>26</sup> and the massive refractivity data sets obtained from the Heuksan-do meteorological observatory<sup>27</sup> are converted into the input parameters for the AREPS software. The conceptual simulation geometry between Jeung-do and Heuksan-do transceivers including these parameters can be depicted as shown in Figure 8, where Tx and Rx are located at the heights of  $h_{Tx}$  (100 m) and  $h_{Rx}$  (249 m) along a distance of  $R_0$  (78 km). Furthermore, to better understand the duct effects on the wave propagation, the seasonal path losses are obtained according to the presence or absence of atmospheric ducts and are compared with each other. Figure 9A-D illustrate the statistical histograms of the path losses at the Rx for all seasons with and without ducts indicated by blue and red bars. In addition, to derive the quantitative means and variances depending on the presence or absence of the ducts, these histogram results are fitted by Burr Type XII PDF curves, as in following formulas<sup>28</sup>:

$$f(x) = \frac{ck \left(\frac{x}{s}\right)^{c-1}}{s \left[1 + \left(\frac{x}{s}\right)^c\right]^{k+1}}, (s, c, k, x > 0), \quad (2)$$

$$\mu = sk\beta \left(\frac{ck-1}{c}, \frac{c+1}{c}\right), \quad (3)$$

$$\sigma = -\mu^2 + s^2 k\beta \left(\frac{ck-2}{c}, \frac{c+2}{c}\right). \quad (4)$$

In the formulas,  $f(x)$  is the Burr Type XII PDF of  $x$ , where  $s$ ,  $c$ , and  $k$  are the parameters that determine the shape and scale of the PDF. The symbols  $\mu$  and  $\sigma$  are the mean and variance of the PDF, which are calculated using the beta function of  $\beta(X, Y)$ . The detailed parameter values of  $s$ ,  $c$ , and  $k$  that are obtained from the four seasons with and without ducts are listed in Table 1. In general case of the duct occurrence, the probability of the low path loss level is

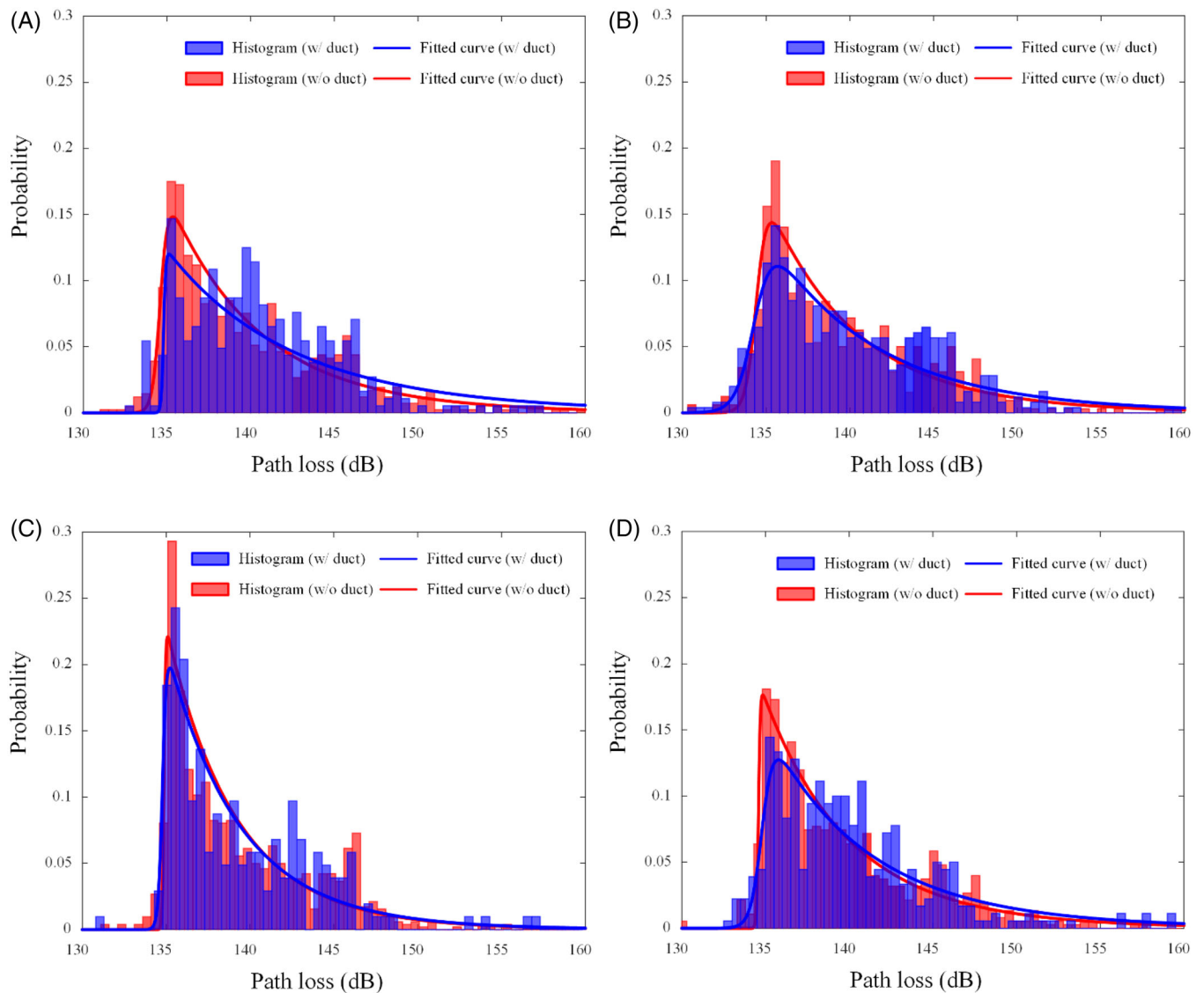


**FIGURE 9** Histograms and fitted Burr Type XII PDF curves of the path loss at Rx for all seasons with and without the duct atmosphere. A, Spring. B, Summer. C, Autumn. D, Winter. PDF, probability density function [Color figure can be viewed at [wileyonlinelibrary.com](http://wileyonlinelibrary.com)]

**TABLE 1** Detailed parameter values

		s	c	k
Spring	w/o duct	134.6	574.8	0.0415
	w/ duct	134.8	1986	0.0086
Summer	w/o duct	134.4	419.6	0.058
	w/ duct	134.3	242.9	0.0829
Autumn	w/o duct	134.6	2480	0.0102
	w/ duct	134.8	401.3	0.0531
Winter	w/o duct	134.9	2829	0.0112
	w/ duct	134.8	1081	0.0281

usually higher than that of the no-duct case, and this phenomenon occurs when the altitude of the duct is close to the height of the Rx. In particular, the abnormal wave propagation can be well observed when both Tx and Rx is inside the duct.

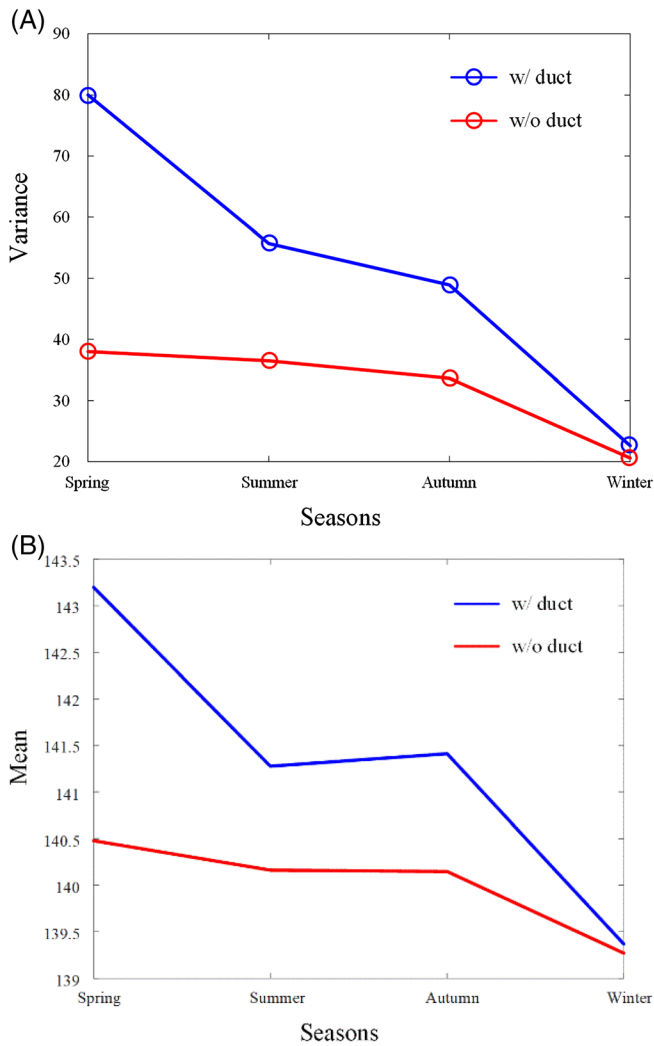
However, according to the results in Figures 9A-D, the probabilities at the low path loss level for the presences of the duct seem to be similar to those of the no-duct cases. It is because hTx and hRx are already determined in our simulation and measurement setup. Especially, since the Rx station is constructed at a high altitude, the surface duct did not have significant effect on the probability result. Therefore, although many duct occurrences were observed in our case, the probabilities of the low path loss in the presences of ducts look similar to those in the no-duct cases.

Figure 10A,B present the variances and means of all seasons according to the presence of the ducts, and the detailed values are listed in Table 2. The variances, in the duct atmosphere, decrease significantly from 80 in spring to 22.6 in winter; comparatively, in non-duct conditions, the maximum and minimum variances of 38 and 20.5 are attained in spring, and the difference of the variances between the with and without the duct decreases from spring to winter. In the absence of

the duct atmospheres, the means are 140.4, 140.2, 140.1, and 139.2 dB for each season, while in the duct conditions the means vary from 143.2 dB in spring to 139.3 dB in winter. These results clearly show that the variation of the path losses

in the duct atmosphere is wider than that of the non-duct atmosphere, so that the abnormal wave propagation characteristics are observed depending on the presence of the duct. In particular, the means and variances between winter duct and non-duct conditions are similar to each other because the number of duct occurrences is minimum compared to other seasons, which barely affects the wave propagation.

To verify the suitability of the simulated path loss in the proposed analysis, real-time measurement of the path losses between Jeung-do and Heuksan-do is conducted in October 2017. The measurement is carried out with the Tx and Rx systems consist of a signal generator, a spectrum analyzer, a power amplifier, and antennas. The detailed parameters and values for the measurement setup are listed in Table 3. We



**FIGURE 10** A, Variance of Burr Type XII PDF for all seasons with and without the duct atmosphere. B, Mean of Burr Type XII PDF for all seasons with and without the duct atmosphere. PDF, probability density function [Color figure can be viewed at wileyonlinelibrary.com]

**TABLE 2** Detailed values of means and variances

		Spring	Summer	Autumn	Winter
Mean	w/ duct	140.5	140.2	140.1	139.3
	w/o duct	143.2	141.3	141.4	139.4
Variance	w/ duct	40	36.5	33.6	20.6
	w/o duct	80	55.7	48.9	22.6

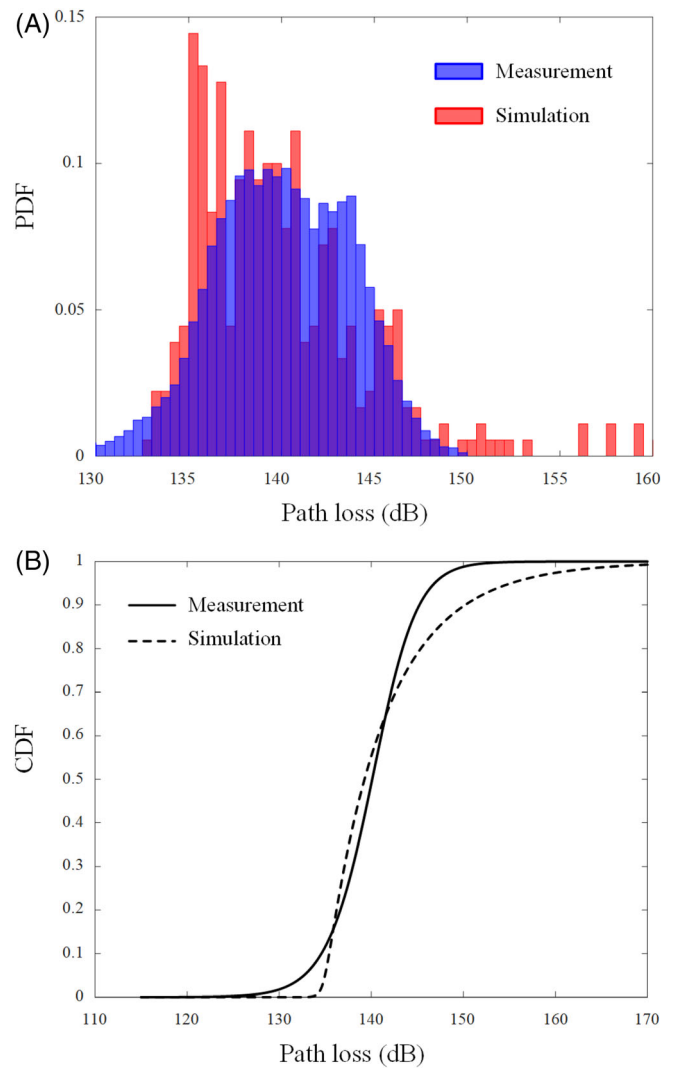


**FIGURE 11** Measured and simulated path loss results in autumn. A, PDF histogram. B, CDF curve. PDF, probability density function [Color figure can be viewed at wileyonlinelibrary.com]

**TABLE 3** Detailed values of the measurement setup parameters

Parameters	$h_{Tx}$ (Jeung-do)	$h_{Rx}$ (Heuksna-do)	$R_0$	Antenna gain	Frequency	Total Tx power	# of measured data
Values	100 m	249 m	78 km	10 dBi	2.58 GHz	53.56 dBm	12 483

also simulate the path losses by applying the 9-year autumn reflective index data sets to the AREPS software as shown in Figure 11A,B. The measurements and simulations are provided with the statistical histograms and fitted curves from Burr Type XII CDF. The measured and simulated results of the histograms have a slight difference due to limitations of the AREPS software that cannot include the system parameters such as a system noise, a total system input power, and the detailed regional refractivity, but the measured CDF curve is better in agreement with the simulation.

## 4 | CONCLUSION

We have investigated the number of duct occurrences in Korean coastal area by the statistical histogram for each season using massive atmospheric data sets assembled from 2010 to 2017 at four meteorological observatories. In the summer result, the maximum number of the duct occurrences was observed to be 1639 higher than in the other seasons. On the other hand, in winter, the minimum number of ducts occurrences was 612 of 4468 winter data sets. The simulated histograms of seasonal path losses were obtained using the AREPS software, and the results were fitted by using Burr Type XII PDF curves. In the duct atmosphere, the variances were reduced from 80 in spring to 22.6 in winter, and the means decreased from 143.2 dB in spring to 139.3 dB in winter. By contrast, in non-duct conditions, the variances and means were varied slightly, where the maximum and minimum variance values were 38 and 20.5, and those of means were 140.4 and 139.2 dB, respectively. Finally, the path loss measurements between Jeung-do and Heuksan-do were carried out in October 2017 and were provided by histograms and Burr Type XII CDF curves, which are in good agreement with the simulations.

## ACKNOWLEDGMENTS

This work was supported by a grant-in-aid from Hanwha Systems, and an Institute for Information & Communications Technology Promotion (IITP) grant funded by the Korean government (MSIP) (No.2017-0-00066, Development of time-space based spectrum engineering technologies for the preemptive using of frequency), and the atmospheric data were supported by Korea Meteorological Administration.

## ORCID

Hosung Choo  <https://orcid.org/0000-0002-8409-6964>

## REFERENCES

- [1] Leeper DG. A long-term view of short-range wireless. *Computer*. 2001;34(6):39-44.
- [2] Panagopoulos AD, Arapoglou PM, Cottis PG. Satellite communications at KU, KA, and V bands: propagation impairments and mitigation techniques. *IEEE Commun Surv Tutor*. 2004;6(3):2-4.
- [3] Wang H, Fapojuwo AO. A survey of enabling technologies of low power and long-range machine-to-machine communications. *IEEE Commun Surv Tutor*. 2017;19(4):2621-2639.
- [4] Skolnik M. *Radar Handbook*. 3rd ed. New York: Mc-Graw-Hill; 2008.
- [5] Nathanson FE. *Radar Design Principles – Signal Processing and the Environment*. 2nd ed. New Jersey: SciTech Publishing; 1999.
- [6] Chou YH, Kiang JF. Ducting and turbulence effects on radio-wave propagation in an atmospheric boundary layer. *Prog Electromagn Res B*. 2014;60:301-315.
- [7] Skolnik MI. *Introduction to Radar Systems*. 3rd ed. New York: Mc-Graw-Hill; 2001.
- [8] Mentis Ş, Kaymaz Z. Investigation of surface duct conditions over Istanbul, Turkey. *J Appl Meteorol Climatol*. 2007;46(3):318-337.
- [9] Wagner M, Gerstoft P, Rogers T. Estimating refractivity from propagation loss in turbulent media. *Radio Sci*. 2016;51(2):1876-1894.
- [10] Gerstoft P, Rogers LT, Krolik JL, Hodgkiss WS. Inversion for refractivity parameters from radar sea clutter. *Radio Sci*. 2003; 38(3):1-22.
- [11] Karimian A, Yardim C, Gerstoft P, Hodgkiss WS, Barrios AE. Refractivity estimation from sea clutter: an invited review. *Radio Sci*. 2011;46(6):1-16.
- [12] Zhao X. “Refractivity-from-clutter” based on local empirical refractivity model. *Chin Phys B*. 2011;27(12):1-5.
- [13] Zhao X, Huang S. Estimation of atmospheric duct structure using radar sea clutter. *J Atmos Sci*. 2011;27(12):1-5.
- [14] Karimian A, Caglar Y, Hodgkiss WS, Gerstoft P, Barrios AE. Estimation of radio refractivity using a multiple angle clutter model. *Radio Sci*. 2012;47(3):1-9.
- [15] Cheng Y, Zhou S, Wang D, Lu Y, Yao J. Statistical characteristics of the surface ducts over the South China Sea from GPS radio-sonde data. *Acta Oceanol Sin*. 2015;34(11):63-70.
- [16] Zhang JP, Wu ZS, Zhao ZW, Zhang YS, Wang B. Propagation modeling of ocean-scattered low elevation GPS signals for maritime tropospheric duct inversion. *Chin Phys B*. 2012;21(10):1-14.
- [17] Lowry AR, Rocken C, Sokolovskiy SV, Anderson KD. Vertical profiling of atmospheric refractivity from ground-based GPS. *Radio Sci*. 2002;37(3):1-21.
- [18] Rogers LT. Effects of the variability of atmospheric refractivity on propagation estimates. *IEEE Trans Antennas Propagat*. 1996; 44(4):460-465.
- [19] Sirkova I. Brief review on PE method application to propagation channel modeling in sea environment. *Cent Eur J Eng*. 2012;2(1): 19-38.
- [20] Shi Y, Yang KD, Yang YX, Ma YL. Experimental verification of effect of horizontal inhomogeneity of evaporation duct on electromagnetic wave propagation. *Chin Phys B*. 2015;24(4):1-9.
- [21] Advanced Refractive Prediction System (AREPS), The Space and Naval Warfare System, San Diego, CA. Version. 3.6, 2005

- [22] Patterson WL, Hitney HV. Radio physical optics CSCI software documents. NCCOSC RDTE DIV Technical Document 1992; 2403.
- [23] Thomson DJ, Chapman NR. A wide-angle split-step algorithm for the parabolic equation. *J Acoust Soc Am*. 1983;74(6):1848-1854.
- [24] Hitney HV. Hybrid ray optics and parabolic equation methods for radar propagation modeling. *IEE Conf Radar*. 1992;365:58-61.
- [25] Meijering E. A chronology of interpolation: from ancient astronomy to modern signal and image processing. *Proc IEEE*. 2002; 90(3):319-342.
- [26] Google, Inc., Google Earth Software, <http://earth.google.com/> Accessed March 31, 2019.
- [27] Korea meteorological Administration "Rawin sonde, <https://data.kma.go.kr> Accessed March 31, 2019
- [28] Zimmer WJ, Keats JB, Wang FK. The Burr XII distribution in reliability analysis. *J Qual Technol*. 1998;30(4):386-394.

**How to cite this article:** Lim TH, Wang S, Chong Y-J, Park YB, Ko J, Choo H. High altitude ducts causing abnormal wave propagation in coastal area of Korea. *Microw Opt Technol Lett*. 2020;62: 643–650. <https://doi.org/10.1002/mop.32079>